

Assessment of a fire-damaged concrete overpass: the Verona bus crash case study

Verona bus
crash and fire

Roberto Felicetti

Civil and Environmental Engineering, Politecnico di Milano, Milan, Italy

293

Received 5 June 2021
Revised 3 October 2021
Accepted 11 November 2021

Abstract

Purpose – This study aims to develop an assessment strategy for fire damaged infrastructures based on the implementation of quick diagnostic techniques and consistent interpretation procedures, so to determine the residual safety margin and any need for repair works.

Design/methodology/approach – In this perspective, several tailored non-destructive test (NDT) methods have been developed in the past two decades, providing immediate results, with no need for time-consuming laboratory analyses. Moreover, matching their indications with the calculated effects of a tentative fire scenario allows harmonizing distinct pieces of evidence in the coherent physical framework of fire dynamics and heat transfer.

Findings – This approach was followed in the investigations on a concrete overpass in Verona (Italy) after a coach violently impacted one supporting pillar and caught fire in 2017. Technical specifications of the vehicle made it possible to bound the acceptable ranges for fire load and maximum rate of heat release, while surveillance video footage indicated the duration of the burning stage. Some established NDT methods (evaluation of discolouration, de-hydroxylation and rebar hardness) were implemented, together with advanced ultrasonic tests based on pulse refraction and pulse-echo tomography.

Originality/value – The results clearly showed the extension of the most damaged area at the intrados of the box girders and validated the maximum heating depth, as predicted by numerical analysis of the heat transient ensuing from the localized fire model.

Keywords Fire damage assessment, Fire scenario models, Non-destructive testing, Ultrasonic testing

Paper type Research paper

1. Introduction

Bridge fires are becoming an increasing concern, due to the development of ground shipping and the high incidence of hazardous transports (Garlock *et al.*, 2012). Though far less frequent than fires in buildings, such events imply a remarkable risk, because of the high costs of service disruption and structural rebuilding or repair. The most severe cases reported in the literature (Peris-Sayol *et al.*, 2017) were caused by accidents involving tanker trucks transporting highly flammable fuels, leading to collapse or demolition of the structure due to excessive deformation (steel and composite decks) or generalized spalling (concrete decks). Less severe damage is generally observed when the fire is fed by just the vehicle components and its fuel.

This was the case of a dramatic collision happened on January 20, 2017, night on the E70 motorway near Verona, Italy. A coach transporting Hungarian high-school students crashed

© Roberto Felicetti. Published by Emerald Publishing Limited. This article is published under the Creative Commons Attribution (CC BY 4.0) licence. Anyone may reproduce, distribute, translate and create derivative works of this article (for both commercial and non-commercial purposes), subject to full attribution to the original publication and authors. The full terms of this licence may be seen at <http://creativecommons.org/licenses/by/4.0/legalcode>

The author wishes to acknowledge Marco Cucchi (Testing Lab for Materials, Buildings and Civil Structures at Politecnico di Milano) for the valuable support during on-site inspections and Nicola Bettini (Di.Mo.Re Strutture) for the cooperative working on the numerical analyses. The author is also grateful to the management of Autostrada Brescia Verona Vicenza Padova for commissioning this assessment work and to Marco Viespoli for the efficient logistical support. A sincere thought goes to the students who lost their lives in this tragic accident and to their families.



into one pillar of a concrete overpass and caught fire (Wikipedia, 2021). Despite the considerable mass of the vehicle (more than 20t) and the high-speed impact (the pillar penetrated 8 m into the chassis), the structure did not exhibit any visible mechanical damage ascribable to the high impulsive load. This evidence was corroborated by numerical stress analyses of the pillar base, showing that in the worst possible scenario the maximum exerted thrust was close to the onset of shear cracking, namely, about 80% of the shear capacity (Belleri *et al.*, 2018).

As concerns fire, the visible signs of damage include spalling on one side of the impacted pillar (with direct exposure of some rebars) and diffuse surface cracking and cover delamination of the above transverse beam.

Due to the considerable thickness of these elements, there was no question they could still resist the design loads and be easily repaired. A more cryptic condition was recognized in the box girders, due to the significant heating of the thin bottom flange in the region sustaining hogging bending moment. The possible damage to post-tensioning cables in the lateral web of the first girder was also at issue.

The preliminary survey suggested a deeper analysis of the heating depth and a reassessment of the residual bearing capacity of the deck. To this purpose, a coordinated procedure was implemented, based on validation of a tentative fire scenario by way of specialized non-destructive testing (NDT) techniques (Felicetti, 2014). The objectives of *in situ* inspections and the adopted techniques can be listed as follows:

- (1) general survey of crack patterns and delaminated/spalled areas (visual inspection and hammer tapping);
- (2) mapping of damage levels at the deck intrados (ultrasonic pulse velocity [UPV] and pulse-echo tomography);
- (3) assessment of damage depth in the most impacted regions (UP refraction, alkalinity and colour checks);
- (4) evaluation of the residual response of exposed rebars (Leeb dynamic hardness tests);
- (5) condition check on the elastomeric bearing pads on top of the portal (visual inspection and lab test).

An account of the above activities and the conclusions that were drawn is given in the following sections.

2. Structure description and post-fire visual inspection

The impacted structure is a semi-integral concrete bridge built in 1992 (Figure 1). The deck includes five post-tensioned box girders sustained by two intermediate precast portals and restrained by sets of six columns at the abutments. Each girder is made of four precast segments assembled with wet joints and post-tensioned with six concordant cables ($7 \times 0.6'$ strands each). Adjacent girders are connected with shear keys obtained by filling two lateral recesses with non-shrink grout. The ungrouted recess of the side girders translates into a reduced cover of the exposed lateral face (see also Figure 6).

To be mentioned is a note on the original drawings prescribing the addition of a not specified amount of polypropylene fibre to the C40/50 concrete mix (possibly to control early age cracking). As will be discussed, this may explain why no spalling was observed on these elements.

The precast portals consist of two inverted tapered pillars (cross-section 0.6×1.1 m to 0.7×1.5 m) and a transverse beam with 1.5 m deep trapezoidal cross-section (width 0.7–1.0 m). The moment resisting connections are obtained by grouting groups of 7×26 mm rebars protruding from each corner of the pillars and inserted in vertical ducts at the edges of the beam.

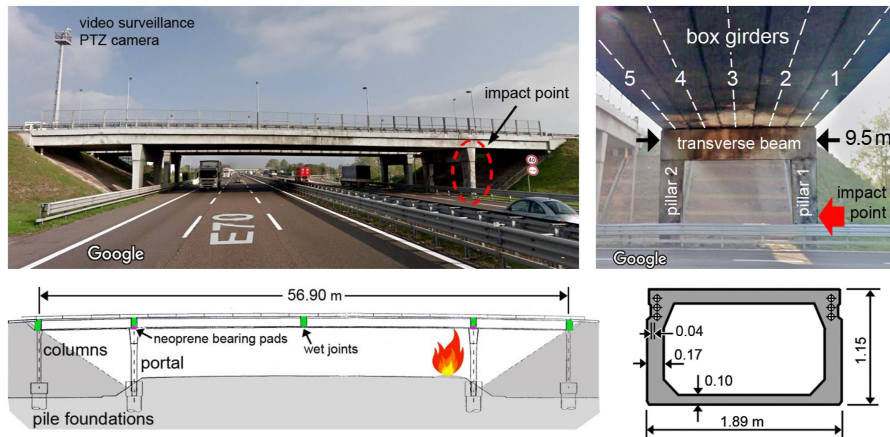


Figure 1.
General views of the
overpass under study,
elements nomenclature
and size

In all elements, fire protection of the reinforcement is provided by a rather thick cover (axis distance of stirrups = 35 mm, minimum surface distance of cables at the lateral recess = 40 mm, Figures 1 and 6).

The visible damages observed during preliminary inspection (Figure 2) include spalling on the upper half of Pillar 1, with direct exposure of two longitudinal rebars and some stirrups (then, a small share of the member reinforcement). A stable delamination of large plates (10–15 mm thick) was recognized at the top of Pillar 2. Here the fractured debris could be easily removed and inspected for discolouration. Extensive incipient delamination was detected by hammer tapping also at the intrados of the transverse beam, together with regularly spaced vertical cracks with the same pitch as the stirrups. In summary, no lack of rebar protection affected these latter two elements.

Despite the direct impact of flames, the intrados of the box girder showed no sign of spalling and just limited delamination, exhibiting a sound response to the tap test. Structural analysis under dead loads showed that the compressive stress borne by the bottom flange next to the support was 5 N/mm^2 , outlining a more favourable condition for spalling compared to the top section of the pillars (average sustained stress 2 N/mm^2). This highlights the likely benefit brought in by polypropylene fibre in the most critical part of the structural system.

A last aspect deserving attention was the possible damage undergone by the elastomeric bearing pads laid between the transverse beam and the box girders. Visual inspection showed a charred surface on the most exposed sides (Figure 3). However, carving a thin slice was sufficient to expose an intact material with a rubbery consistency. In a laboratory test, a identical pad was stacked between concrete cubes and exposed to 30-min intense radiant heating (about 50 kW/m^2). The specimen showed limited charring depth (4 mm) and decreasing heating rate, due to the protective effect of the charred layer and the high conductivity of the reinforcing metal shims. The maximum temperature at 10-mm depth was below the onset of decomposition as indicated by thermogravimetric analysis (Caballero *et al.*, 2005), confirming the good fire endurance of this component.

3. Accident details, fire scenario and thermal analyses

The technical specifications of the burnt coach are summarized in the table in Figure 4. The diesel fuel was contained in two tanks anterior to the front wheels, one of which was destroyed by the impact. A supplementary tank was also installed in the central part of the chassis. The surveillance camera installed across the highway (Figure 1) was not framing the accident area, but the impact instant was indicated by image blurring due to vibration of

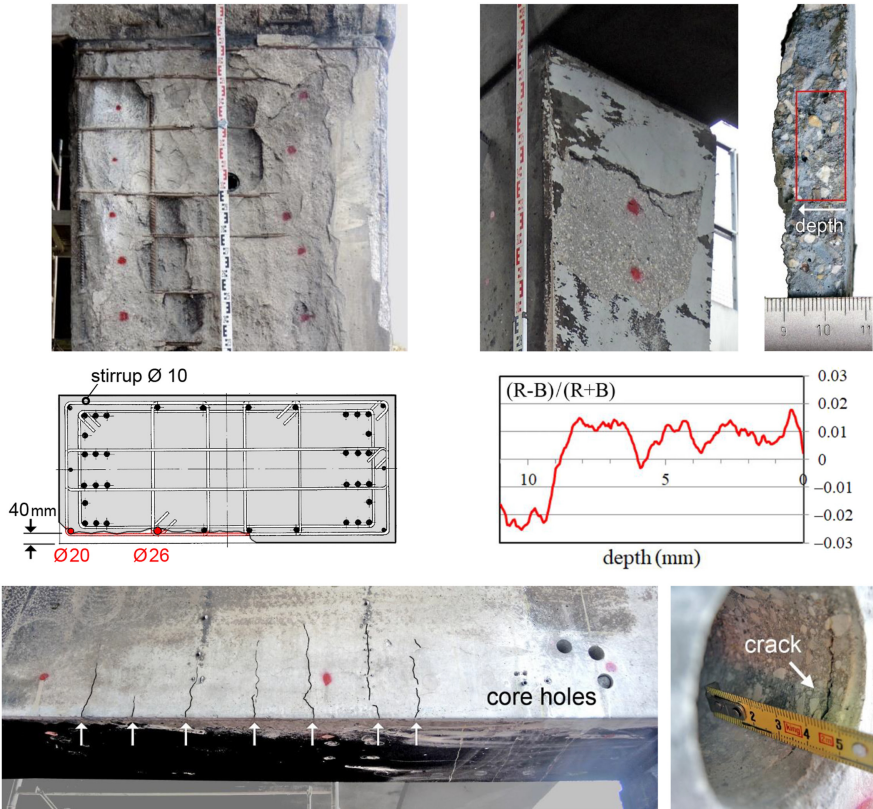


Figure 2. Observed damage patterns: spalling at the top of Pillar 1; stable delamination at the top of Pillar 2 and discoloration of a detached plate; equally spaced cracks and incipient delamination at the bottom chord of the transverse beam

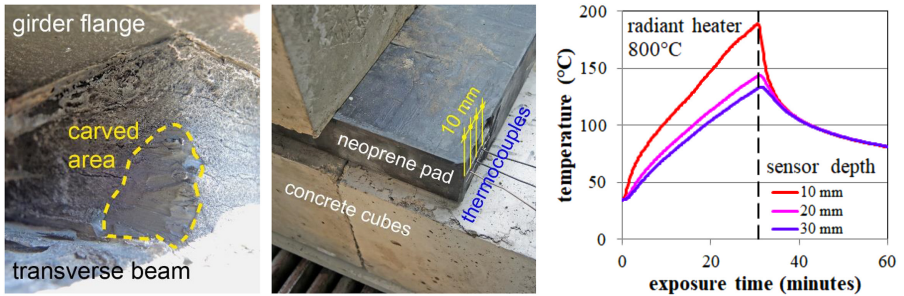


Figure 3. Charred skin removal from a neoprene bearing pad and heating curves resulting from the radiant heater test

the supporting pole. Later, the camera was directed towards the vehicle, though the view was obstructed by the overpass deck. Nonetheless, it was possible to spot some smoke 3 min after the impact and long flames sticking out the parapets 1 min later. Pictures and videos shot by witnesses recorded the flame height (Figure 5). Two fire engines reached the place 16 min after the accident and flame extinction was completed about 15 min later.

Based on the above indications and data from the literature (Beard and Carvel, 2012), a possible trend of the heat release rate (HRR) curve was sketched, according to the following assumptions:

- (1) ultra-fast parabolic growth (t -squared model, 1 MW in 75s);
- (2) 40 MW maximum power (by scaling literature data to the larger number of seats and fire load);
- (3) 30 min total duration of the fire event (video footage).

The total released energy entailed by this scheme adds up to nearly 50 GJ.

The HRR curve was introduced in the Hasemi's model of localized fire (EN, 1992-1-2, 2002) with a diameter of 5 m and fire-to-soffit height of 4 m. Given the vehicle slenderness (length/width = 5.5) and the lower intensity of flames at its front (Figure 5), the assumed burning area was slightly undervalued. Due to the high thermal power, the condition where flames directly impinge the structure was met for 80% of the fire duration and the received heat flux approached the maximum value allowed by the model. This made the results insensitive to possible adjustments of the HRR curve.

The ensuing heat flux was then used to implement the thermal analysis of the key parts of the structure: a 100-mm thick plate representing the box girder flange at the intrados and the recess zone on the lateral side of the first girder. The recess zone was analysed by way of a 2D finite element model (Figure 6), where the cable was regarded as a homogeneous disk whose thermal properties were the average of steel and grout properties weighted on their respective cross-section areas. The beam intrados was also modelled by means of a 1D finite-difference routine, as a starting point for the following reconstruction of ultrasonic refraction ray paths (section 5).

The analyses were continued until all nodes in the discretized models had reached the cooling stage (Colombo and Felicetti, 2007), so to determine the maximum temperature ever experienced at each point, to be related to the unrecoverable damage detected by way of non-destructive inspections. It can be observed that this rather intense but short fire is expected not to cause a very deep heating of the exposed members. Moreover, the thermal bridge produced by a cable fosters the gradient in the cover and keeps the most exposed side of the duct colder compared to a plain concrete element (the rebar-centre rule applies also to thicker reinforcement).

vehicle specifications

- brand/model: Setra S317 GT-HD
(3 axles, High Decker, 17 seat rows)
- length: 13.850 m
- width: 2.500 m
- height: 3.615 m
- gross mass: 24000kg
- additional ski box: 650kg
- tank capacity: 480 + 370 litres
- occupants: 54 passengers + 2 drivers

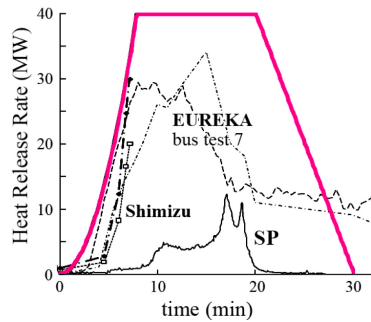


Figure 4. Technical specifications of the coach and assumed HRR curve compared against results from the literature



Figure 5. Pictures showing the flame height in the fully developed stage of the fire

4. General mapping of damage at the deck intrados

The first task in the framework of onsite inspections was recognizing the most heated zones of the bottom flange of the box girders, which were directly impinged by the flames but experienced just minor delamination. This aspect looked not crucial in the precast portal, since extensive cracking affected the member's surface, requiring a complete reinstatement of the concrete cover.

The option of surface hardness survey by means of the rebound hammer was discarded, due to the limited thickness of the plates and the poor sensitivity to fire damage of this method (Felicetti, 2014). A definitely more responsive material property is the velocity of ultrasonic pulses (UPV), to be monitored with the probes side by side on the exposed face of the elements (indirect method, Bungey *et al.*, 2006), being the hollow core of the girders not accessible. To this purpose, a rubber template was devised (Figure 7), so to keep the ultrasonic probes at 150 mm centre-to-centre distance, with full adaptability to any surface unevenness and no cross-talk. In actual fact, the effective distance was 13.7 mm less, due to the not negligible probe size (30 mm diameter), which implies an inherent offset (Bungey *et al.*, 2006). As will be

Figure 6. FE model of the recess region of the girder and maximum temperature envelope profiles in the cable and its cover

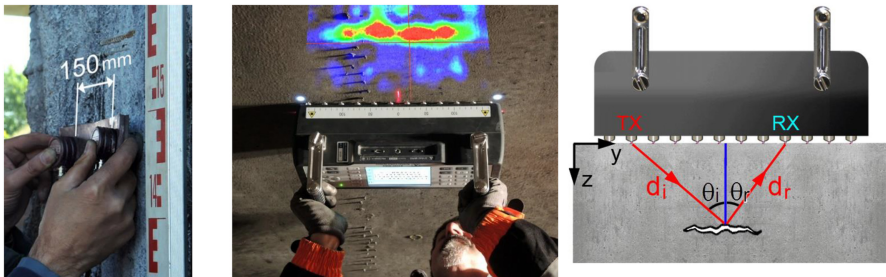
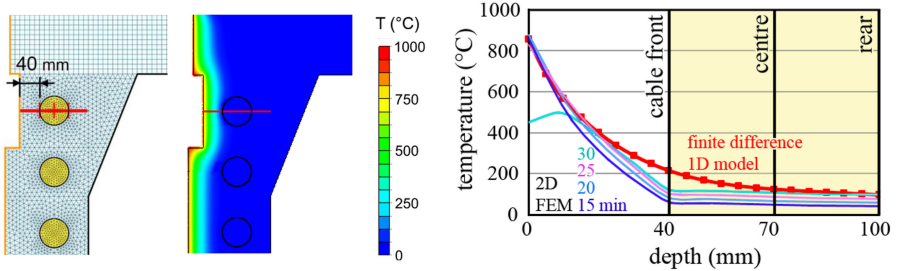
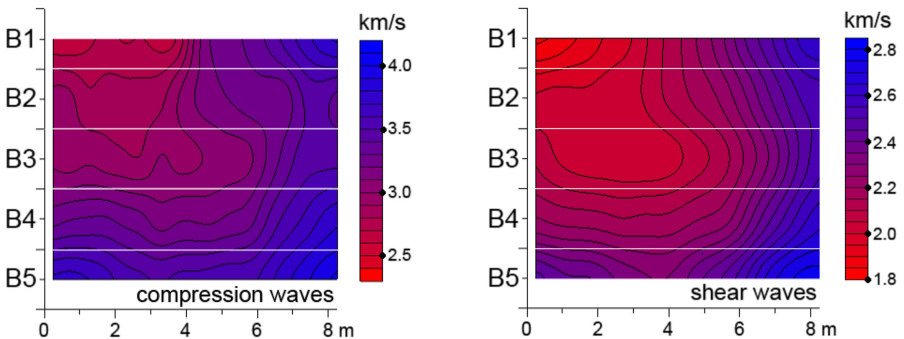


Figure 7. Setup for fast UPV mapping via the indirect method and the A1040 MIRA tomograph; their respective pulse velocity maps detected at the intrados of the five box girders composing the deck (abscissa measured from the portal edge)



more deeply discussed in the next section, the selected distance allows an optimal balance between sensitivity to thermal damage and signal strength.

This setup was used to scan the central axis of the girders flange (0.5 m step) and several vertical alignments along the pillars (0.25 m step) and horizontal sections along the transverse beam (0.5 m step). The results pertaining to the deck intrados were collected in the form of a map (Figure 7), clearly illustrating the remarkable pulse velocity reduction in the area right above the burnt coach. Damage tends to vanish at a distance exceeding 8 m from the portal edge and in the farthest beam. It has to be stressed that the minimum indicated values represent the mean pulse velocity along a curved ray path plunging to about 20 mm in the damaged cover (see the wavefront trajectories in Figure 10).

An alternative way to map the surface condition is represented by an innovative ultrasonic tomograph (A1040 MIRA by Acoustic Control Systems, Figure 7) based on the pulse-echo principle (Bellanova *et al.*, 2017). The equipment is fitted with an array of 12 sensors working in turn as transmitters (TX) or receivers (RX). The transmitter sends a short ultrasonic pulse which is reflected by any void or strong inhomogeneity in the material and then is detected by a receiver. Under the assumption of a uniform propagation velocity, the delay of the received pulse indicates the total distance ($d_i + d_r$) covered by the incident and the reflected waves. The process is repeated for all possible combinations of sensors pairs (66 waveforms collected in about 2 s) and the signals are processed according to the Synthetic Aperture Focusing Technique (Schickert *et al.*, 2003), so to produce an image of reflectors across a section orthogonal to the tested surface (B-scan). Other peculiar features of this instrument are the spring-loaded dry-point contact sensors, not requiring any coupling medium to adapt to the surface unevenness, and the use of shear wave pulses, characterized by a lower velocity and not suffering any mode conversion when reflected.

In the application at issue, the steep gradients of pulse velocity tend to invalidate the SAFT algorithm and the strong bottom-echo produced by the inner cavity of the girders progressively vanishes as fire damage increases (Figure 8). Nonetheless, the slower surface layer tends to

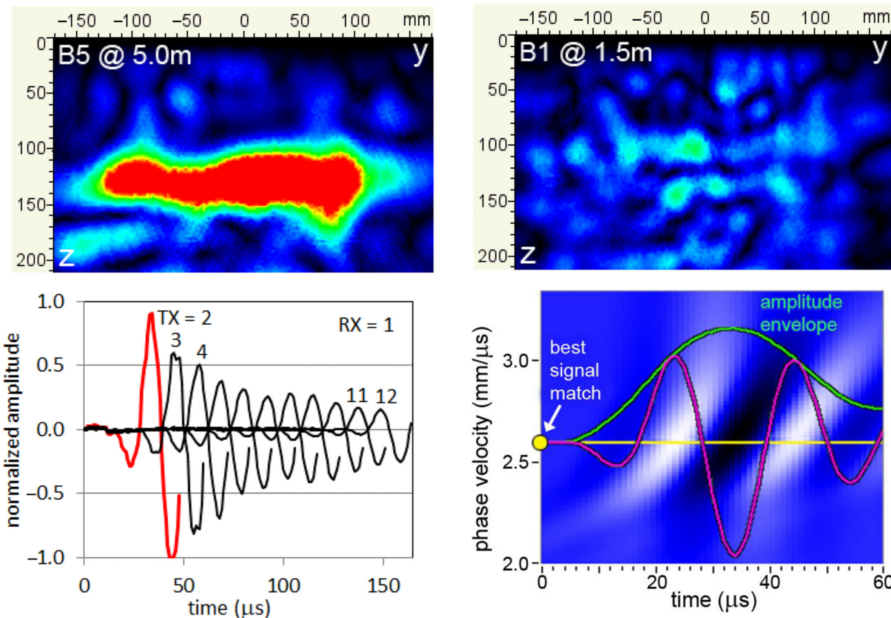


Figure 8. Different strength of the bottom-echo in case of pristine and damaged concrete flanges, regular increase of arrival time at the increasing transmitter–receiver distance, assessment of surface wave velocity by optimization of the pulse alignment

guide horizontally polarized shear waves (Love waves), which propagate along the surface with milder decay compared to other modes. This mode governs the first received signal, whose time shift goes with the sensor spacing divided by the surface wave velocity. The latter parameter is determined by optimizing the pulse realignment (max waveform sum).

Besides the different magnitude (shear waves are 40% slower than compression waves), the resulting map (Figure 7) is very similar to the one obtained by means of the traditional UPV method. However, merging 66 waveforms in one measurement allows offsetting the local disturbance due to cracks, rebars and other defects, producing a smoother output. To be mentioned is that both mapping techniques were implemented at the pace of 25 test points per hour, minimizing the traffic disruption in this strategic highway.

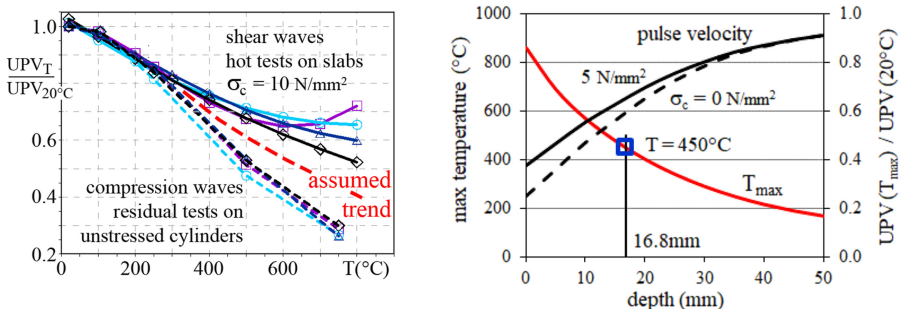
5. Validation of damage depth by ultrasonic pulse refraction

The velocity of elastic waves is one of the most responsive indicators of concrete thermal damage, due to the pronounced temperature sensitivity of the Young's modulus and to the synergistic effect of drying (Colombo and Felicetti, 2007). Nonetheless, a mild compressive loading may mitigate this effect, as a result of the reduced meso-scale damage at the aggregate-cement interface (Figure 9, Felicetti and Lo Monte, 2016). This aspect should be duly considered when dealing with columns or the compressed chord of beams, since a more severe temperature exposure may be inferred from the observed response.

Due to the steep temperature variations induced by fire, remarkable velocity gradients develop in the concrete cover, which behaves like a strongly layered medium. Though scaled down by 3–4 orders of magnitude, the problem resembles a natural soil whose mechanical properties improve with depth. Taking inspiration from Geophysics, the velocity profile can be characterized via the refraction of ultrasonic compression (P) waves implemented by way of the indirect UPV technique. In this method, the measurement of the pulse time-of-flight is performed by applying both the emitting and receiving probes on the same face of the investigated element (Figure 10). When the material velocity rises with depth, the first wavefront detected by the receiver follows a curved ray path representing the best compromise between a shallow trajectory of shorter length and a deeper route involving faster-undamaged layers (Felicetti, 2013). As a consequence, the maximum explored depth is a function of the probe distance X. A series of repeated time-of-flight measurements at increasing probe distance allows to sound deeper and deeper layers in the cover. The outcome is an X-t plot whose shape has been the object of several studies in the literature (Greenhalgh and King, 1981). To be recalled among its properties:

- (1) A monotonically increasing velocity profile implies a convex shape. Any exception indicates the presence of cracks, which should be avoided by preliminary visual inspection and hammer tapping.

Figure 9. Thermal decay of Ultrasonic Pulse Velocity as a function of the sustained stress (Felicetti and Lo Monte, 2016); profiles of the max temperature and corresponding UPV for a 100 mm thick plate submitted to the localized fire as per §3 (including the depth of the 450 °C isotherm detected by the dehydroxylation test)



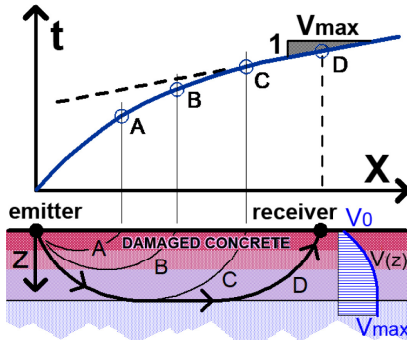
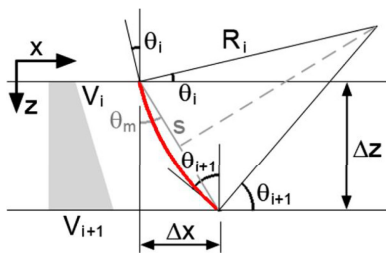


Figure 10. Basic principle of the pulse refraction method, application to the intrados of a box girder, circular ray path in a generic layer with linear velocity trend and formulas for the incremental construction of the X-t curve



Snell's law: $\sin(\theta)/V = p = \text{ray parameter (constant)}$
 for any p in the range $1/V_{\max} \leq p \leq 1/V_0$ find θ_i and θ_{i+1}
 $\Delta x = \Delta z \cdot \tan[(\theta_{i+1} + \theta_i)/2] = \Delta z \cdot \tan(\theta_m)$
 $R_i = \Delta z / [\sin(\theta_{i+1}) - \sin(\theta_i)] = \Delta z / [p \cdot (V_{i+1} - V_i)]$

propagation time:
 $\Delta t_i = \int R_i/V d\theta = R_i \cdot p \cdot \int 1/\sin(\theta) d\theta$
 $= R_i \cdot p \cdot \{\ln[\tan(\theta_{i+1}/2)] - \ln[\tan(\theta_i/2)]\}$
 if $V_i = V_{i+1}$ then $R_i = \infty$ and $\Delta t_i = 2 \Delta z \cdot p / \sin(2\theta)$

- (2) The local slope at any point equals the slowness of the deepest layer crossed by the corresponding minimum-time ray path (slowness = 1/velocity). Then, the curve asymptotically tends to a linear trend whose slope is the slowness of the deepest undamaged layer (maximum velocity and minimum slope).
- (3) The rate of convergence to the final linear trend denotes the thickness of the damaged layer: a higher asymptote intercept indicates a delayed convergence and then a deeper damage.

A systematic series of numerical simulations of different thermal transients involving a broad range of concretes allowed us to derive some correlations (Felicetti, 2013) between these geometrical features and the underlying material damage (inverse problem). As an alternative, the theoretical X-t curve can be easily plotted once a guess velocity profile is determined by combining the material decay curve (Figure 9) and the maximum temperature experienced at each depth, as results from the analysis of the thermal transient ensuing from a tentative fire scenario (cooling stage included).

To this purpose, the cover is discretized in a series of layers with linearly changing velocity through their thickness Δz (Figure 10). In each layer, a ray path obeying the Snell's law of wave refraction takes the shape of a circular arc whose radius depends on the velocity gradient (Greenhalgh and King, 1981). The increments of covered distance ΔX and time-of-flight Δt are expressed in closed form and can be summed across the explored thickness. The following hints should be considered in the implementation of this scheme:

- (1) If $V(z)$ is not monotonically increasing the formulae in Figure 10 are still valid, with $R < 0$.
- (2) A ray path of initial angle θ_0 can re-emerge if $\arcsin(V_0/V_{\max}) \leq \theta_0 \leq \pi/2$, and then $1/V_{\max} \leq p \leq 1/V_0$.

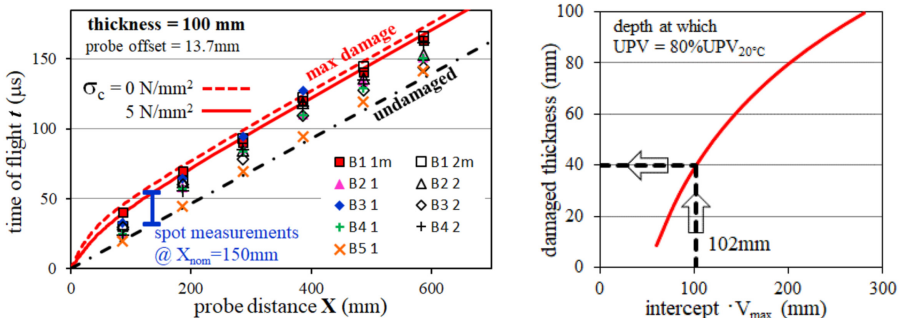
- (3) For any ray parameter p in the above range, the inversion point $\theta = \pi/2$ is at the depth, where $V = 1/p$.
- (4) Ray paths of gradually increasing initial slope (decreasing θ_0 and p) lead to deeper inversion points and milder slopes on the $X-t$ curve. However, X and t are monotonically increasing functions of $1/p$ only in the case of a convex velocity profile ($d^2V/dz^2 \leq 0$). If this condition is not met, multiple arrival times are obtained for the same distance X (triplication) and the shortest time envelope should be considered.

The above procedure was implemented with reference to the localized fire scenario depicted in Section 3. The maximum temperature envelope profile (Colombo and Felicetti, 2007) within the 100-mm thick bottom flange of the box girders was calculated via a 1D finite-difference procedure, which was continued until all terms in the temperature vector had reached the cooling stage. The velocity profile was then obtained, based on the expected decay for slightly compressed concrete (reference pulse velocity for pristine concrete $V_{20^\circ\text{C}} = 4.3$ km/s). The intermediate curve in Figure 9 was adopted, being about 5 N/mm^2 the average compressive stress sustained by the bottom flange under dead loads. Finally, the refracted ray paths and the corresponding $X-t$ curve were traced by keeping the same discretization as the thermal model (Figure 11).

In situ measurements were taken along the central axis of each box girder, at a 1 and 2 m distance from the edge of the supporting transverse beam. The comparison against the theoretical trends (Figure 11) shows that all results lie between the plots pertaining to undamaged concrete (a straight line of slope $1/V_{20^\circ\text{C}}$) and to the maximum expected damage above the localized fire source. A good correspondence is observed between damage depth and the location in the general velocity maps of Figure 7, with smoothly decreasing effects in Beams 4 and 5. The effectiveness of spot measurements at $X = 150$ mm nominal probe distance in discriminating damage levels in this range is also highlighted in the diagram.

It has to be remarked that the theory of waves refraction allows establishing a direct connection between velocity profiles (and then mechanical damage) and field results. This is the basis behind the semi-empirical correlation proposed in Felicetti (2013), providing an indication of the damaged thickness, with no specific assumptions on the fire scenario and the inherent material sensitivity to fire. However, the limited thickness of the flanges under study would require to adapt the proposed relation, since the depth at which a 20% decay of pulse velocity is assigned ($T = 300^\circ\text{C}$, depth ≈ 30 mm in Figure 9) is overestimated by about 10 mm.

Figure 11. Comparison between measured pulse propagation times and the theoretical $X-t$ curve descending from the assumed fire scenario; quick assessment of damage depth according to the semi-empirical correlation proposed in Felicetti (2013)



6. Further checks

The maps of ultrasonic velocity at the deck intrados and the validation of the tentative fire scenario by way of ultrasonic pulse refraction already allowed forming a clear picture of the fire impact on the box girders, whose support region was recognized as the most critical part of the structure. Nonetheless, other inspection techniques were implemented to corroborate this appraisal.

Colorimetry. Some discolouration was visible across the thickness of delaminated plates of Pillar 2 and inside the holes remaining on the transverse beam from former cores extraction (Figure 2). This shift to pink was objectively recognized on digital images by computing the normalized difference between the red and blue colour planes $(R-B)/(R+B)$. This parameter is equivalent but easier to obtain than the strict analysis proposed in Colombo and Felicetti (2007). The alteration (ascribable to heating above 470 °C) was found not to exceed 9 mm depth, which indicates a less severe heating of these two elements compared to the girder intrados, as could be inferred from their smaller view factor.

De-hydroxylation depth. Calcium hydroxide is the main source of alkalinity in concrete pores. It is decomposed by heating above 450 °C, leading to the formation of calcium oxide, which is a highly hygroscopic product. For this reason, the reaction is reversible and can be recognized only if no water is used while sampling, as is made possible by collecting drilling powder via the Carbontest[®] kit (Felicetti, 2013). Tests performed on the portal confirmed the lower impact of fire, as anticipated by colour analysis (max de-hydroxylation depth = 10.5 mm). Checks on the exposed web of the first girder (Figure 12) gave slightly lower values than expected (<15 mm vs 16.8 mm in Figure 9), confirming the assumed fire scenario as a cautious description of the event.

Dynamic hardness tests on rebars. Steel rebars may recover a significant share of their initial strength during cooling, though this strongly depends on their metallurgical features (alloying elements, thermal and mechanical working process – Felicetti *et al.*, 2009). The dynamic hardness test (Leeb method) is a viable tool to assess their residual performance regardless of original quality (Felicetti, 2014). Tests were performed on one rebar exposed by spalling in Pillar 1 and a reference piece uncovered by chiselling on the opposite side. The results (mean rebound index/std deviation = 515/6 and 536/8, respectively) showed a marginal decay of the rebar response (−4%), which corresponds to an almost double loss of yield strength. Given also the minor contribution to the sectional capacity of rebars laid bare by spalling (Figure 2), this confirms the little impact of fire on this element. For Tempcore bars, a permanent loss of strength of about 10% can be ascribed to heating in the range between 600 and 700 °C (Felicetti *et al.*, 2009), which seems coherent with the other observations.

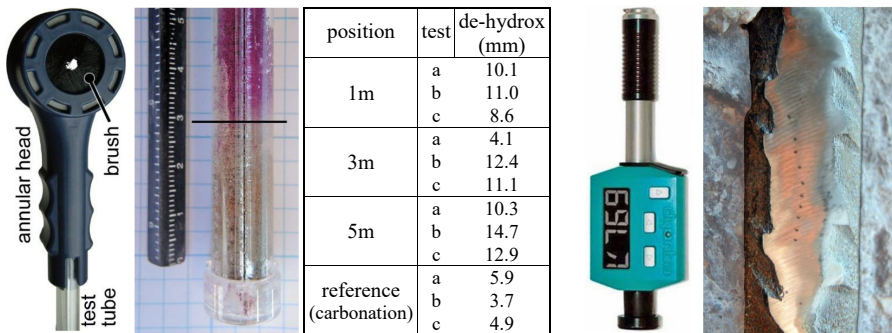


Figure 12. The Carbontest[®] kit, a de-hydroxylated powder sample (scale factor 2.25) and results collected on the exposed web of the first girder; Leeb dynamic hardness tester and resulting indentations on the smoothed face of an exposed rebar of Pillar 1

Reference measurements were also performed on elements not impacted by fire in order to determine the original carbonation depth (about 5 mm, corresponding to the minimum detectable dehydroxylation depth), and the values of compression- and shear-waves velocity in undamaged box girders (4.4 and 2.8 km/s, respectively).

7. Evaluation of residual bearing capacity

As discussed, the massive elements composing the supporting portal underwent shallow heating, diffuse cover delamination and localized spalling, which affected just the residual durability rather than the bearing capacity of the elements. A more critical condition can be recognized at the intermediate support of the box girders, where hogging moment develops, involving compression of the thin bottom flange at the exposed intrados.

The original design of the bridge dates back to the early 1980s when military loads were still considered by the Italian design code. This resulted in a slightly more demanding design hogging moment compared to the current regulations, entailing somewhat oversized cross-sections. As a first step, the profile of post-tensioning cables was digitized in a spreadsheet file and the effect of equivalent tendon loads was introduced in the elastic model of the redundant static scheme of the girder (assumed final/initial tendon stress = 90%, fiction coefficient = 0.2). The results confirmed a negligible effect of post-tensioning on supports, validating the concordant profile of cables. Moreover, the elastic analysis under dead loads allowed assessing the compressive stress borne by the bottom flange during fire (≈ 5 MPa), which mitigates the thermal damage (Figure 9) and fosters the sensitivity to spalling (Lo Monte and Felicetti, 2017). The model was also used to determine the maximum reaction force (≈ 300 kN) which would be possible to exert with a temporary support at midspan in order to unload the same flange during repair works.

Concerning the ultimate capacity of the critical section, the performed investigations led to the conclusion that the post-tensioning cables underwent a non-significant heating (<120 °C, Figure 6), whereas temperature exceeded 300 °C in the first 30 mm of the most exposed cover (temperature profile of Figure 9). Though concrete is expected to retain most of its strength at this reference temperature, stability in the presence of possible fractures and durability in case of increased porosity were also of concern. Then, a check on the residual capacity was performed by neglecting any contribution from this layer. The results showed that the original extra capacity in the hogging bending moment region dropped from +30% to +10% relative to the design bending moment as per the current design regulations (Figure 13). Even though the safety check was passed, the sizeable loss of resisting area caused a rise of the neutral axis at the Ultimate Limit State from 20% to 35% of the cross-section depth, significantly affecting the rotation capacity of the weakest cross-section in this redundant scheme. Some strengthening works were then recommended to the highway management to reinstate the original sectional ductility as well as cover stability.

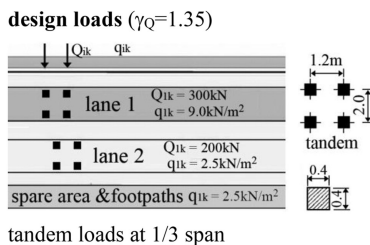
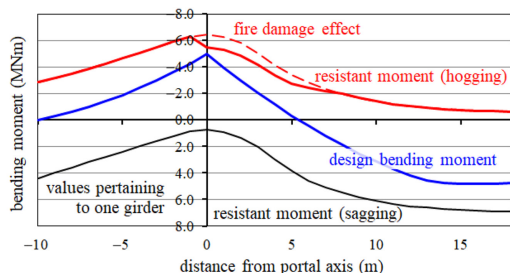


Figure 13.
Design loads and diagrams of the design and resistant bending moments for the most fire-damaged girders



8. Concluding remarks

Case studies in post-fire damage assessment represent an essential opportunity to validate the operational strategies and to verify the viability and effectiveness of both established and innovative inspection tools. The lessons learnt in the analysis of a fire-damaged concrete bridge are briefly summarized here.

Depicting a tentative scenario, and then the ensuing thermal output and the consequent temperature profiles in the exposed members allow a consistent and harmonized interpretation of many distinct indications ensuing from visual inspection and NDT results. A sensitivity analysis is advisable in case of possible alternative assumptions and uncertain parameters.

Several specialized inspection techniques are available, providing immediate indications on some mechanical or chemo-physical features of the material. The alkalinity analysis of drilling powder samples stands out for affordability. Ultrasonic pulse refraction and pulse-echo tomography are to be cited among the advanced tools for a deeper analysis, at the cost of more sophisticated equipment and data processing.

Besides the residual capacity of some critical sections, other features may be at issue, like durability, cover stability, sectional ductility and global robustness of the structural system.

References

- Beard, A. and Carvel, R. (2012), *The Handbook of Tunnel Fire Safety*, 2nd ed., ICE, London.
- Bellanova, M., Cucchi, M., Felicetti, R. and Lo Monte, F. (2017), "Unconventional applications of A1040 MIRA tomograph", *17th Conference of the Italian Association for Non-Destructive Testing (AIPnD)*, October 25-27.
- Belleri, A., Bettini, N. and Felicetti, R. (2018), "Evaluation of the impact and fire damage of a highway bridge", *Proc. of the Italian Concrete Days*, Lecco, 8p, in Italian, available at: <http://hdl.handle.net/10446/125455>.
- Bungey, J.H., Millard, S.G. and Grantham, M.G. (2006), *Testing of Concrete in Structures*, 4th ed., Taylor & Francis, London, New York, p. 353.
- Caballero, J.A., Conesa, J.A., Martín-Gullón, I. and Font, R. (2005), "Kinetic study of the pyrolysis of neoprene", *Journal of Analytical and Applied Pyrolysis*, Vol. 74, pp. 231-237.
- Colombo, M. and Felicetti, R. (2007), "New NDT techniques for the assessment of fire-damaged concrete structures", *Fire Safety Journal*, Vol. 42, pp. 461-472.
- EN 1992-1-2 (2002), *Eurocode 1: Actions on Structures - Part 1-2: General Actions - Actions on Structures Exposed to Fire, Annex C: Localised Fires*, CEN - European Committee for Standardization, Brussels.
- Felicetti, R. (2013), "Assessment methods of fire damages in concrete tunnel linings", *Fire Technology*, Vol. 49 No. 2, pp. 509-529.
- Felicetti, R. (2014), "Assessment of fire damage in concrete structures: new inspection tools and combined interpretation of results", *Proc. 8th Int. Conf. Structures in Fire - SIF 14*, Shanghai (China), pp. 1111-1120.
- Felicetti, R. and Lo Monte, F. (2016), "Pulse-echo monitoring of concrete damage and spalling during fire", *Proc. 9th Int. Conf. Structures in Fire 2016 - SIF16*, Princeton (USA), pp. 851-858.
- Felicetti, R., Gambarova, P.G. and Meda, A. (2009), "Residual behaviour of steel rebars and R/C sections after a fire", *Construction and Building Materials*, Vol. 23 No. 12, pp. 3546-3555.
- Garlock, M., Paya-Zaforteza, I., Kodur, V. and Guc, L. (2012), "Fire hazard in bridges: review, assessment and repair strategies", *Engineering Structures*, Vol. 35, pp. 89-98.

- Greenhalgh, S.A. and King, D.W. (1981), "Curved raypath interpretation of seismic refraction data", *Geophysical Prospecting*, Vol. 29, pp. 853-882.
- Lo Monte, F. and Felicetti, R. (2017), "Heated slabs under biaxial compressive loading: a test set-up for the assessment of concrete sensitivity to spalling", *Materials and Structures*, Vol. 50 No. 192, available at: <https://link.springer.com/article/10.1617/s11527-017-1055-1#citeas>.
- Peris-Sayol, G., Paya-Zaforteza, I., Balasch-Parisi, S. and Alós-Moya, J. (2017), "Detailed analysis of the causes of bridge fires and their associated damage levels", *Journal of Performance of Constructed Facilities*, Vol. 31 No. 3, available at: <https://ascelibrary.org/action/showCitFormats?doi=10.1061%2F%28ASCE%29CF.1943-5509.0000977>.
- Schickert, M., Krause, M. and Muller, W. (2003), "Ultrasonic imaging of concrete elements using reconstruction by synthetic aperture focusing technique", *ASCE Journal of Materials in Civil Engineering*, Vol. 15 No. 3, pp. 235-246.
- Wikipedia, "2017 Verona bus crash", available at: https://en.wikipedia.org/wiki/2017_Verona_bus_crash (accessed May 2021).

Corresponding author

Roberto Felicetti can be contacted at: roberto.felicetti@polimi.it